Electronic Supplementary Information (ESI†)

CeO_2@C derived from benzene carboxylate bridged metal organic frameworks: Ligand induced morphology evolution and influence on the electrochemical properties as lithium-ion battery anode

Sandipan Maiti,[a] Tanumoy Dhawa,[a] Awadesh Kumar Mallik,[b] and Sourindra Mahanty[a,]*

[a]Fuel Cell & Battery Division, CSIR-Central Glass & Ceramic Research Institute, Kolkata 700032 India

[b]Bioceramics & Coating Division, CSIR-Central Glass & Ceramic Research Institute, Kolkata 700032 India

*Correspondence to be addressed to: mahanty@cgcri.res.in; s_mahanty@hotmail.com

Tel: +91-33-2322 3495 Fax: +91-33-2473 0957

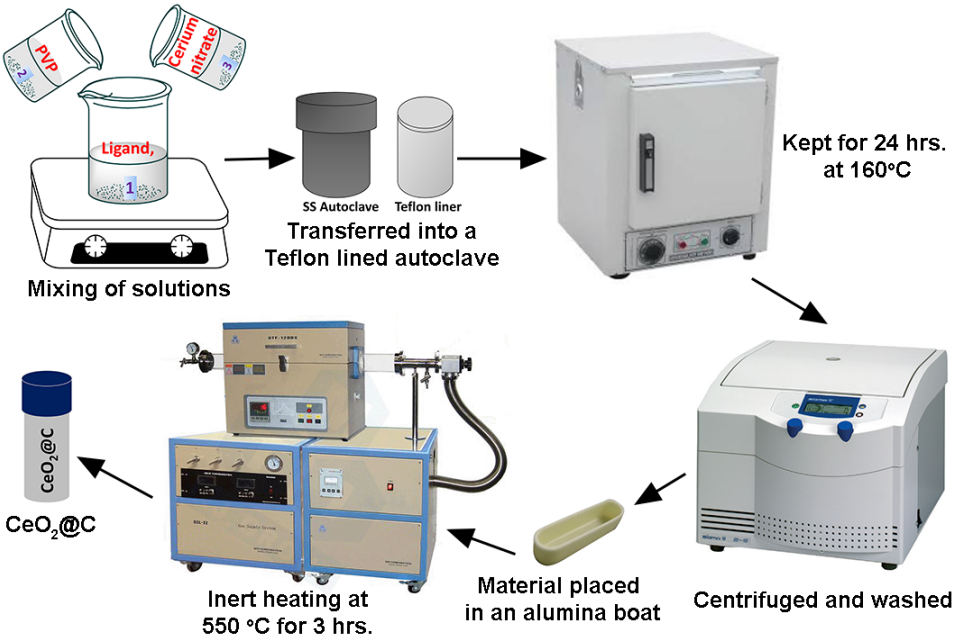

Scheme-S1. A pictorial representation for stepwise synthesis of CeO_2@C.

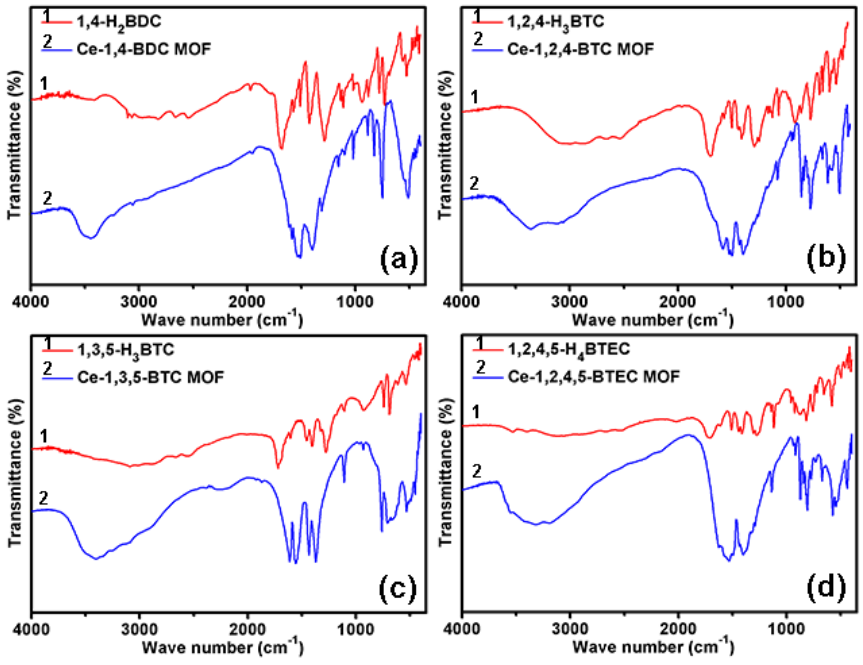

Fig. S1. FTIR spectra of (a) 1,4-H_2BDC & Ce-1,4 BDC MOF, (b) 1,2,4-H_3BTC & Ce-1,2,4 BTC MOF, (c) 1,3,5-H_3BTC & Ce-1,3,5 BTC MOF and (d) 1,2,4,5-H_4BTEC & Ce-1,2,4,5 BTEC MOF

Table-S1. XRD analysis data for MOF derived CeO_2@C

Sample ID	Lattice Constant (Å)	FWHM (Degree)	Crystallite Size (nm)	Lattice Strain
CeO_2@C-14	5.4117(5)	1.38	6.2	0.024
CeO_2@C -124	5.4101(1)	2.04	4.2	0.035
CeO_2@C -135	5.4121(4)	1.59	5.4	0.027
CeO_2@C -1245	5.4274(3)	2.61	3.3	0.045

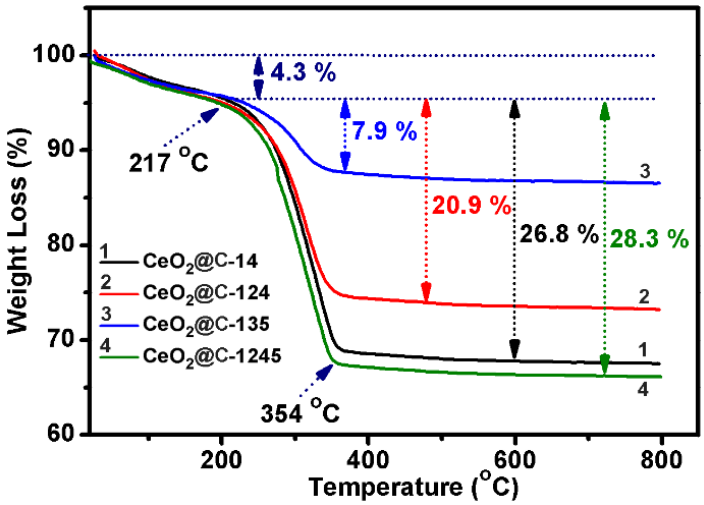

Fig. S2. Thermogravimetric analyses of CeO_2@C-14, CeO_2@C-124, CeO_2@C-135 and CeO_2@C-1245

A variable amount of carbon content has been observed. The carbon content was found to be very low (only 7.9 wt%). in CeO_2@C-135 compared to other samples (20.9-28.3 wt%). This is due to occurrence of an auto-combustion process after annealing in inert atmosphere. As soon as the inert calcined Ce-1,3,5-BTC MOF is removed from the chamber and bring to the ambient atmosphere, an auto-combustion process set-in. This process is more vigorous in case of Ce-1,3,5-BTC MOF and very mild in case of Ce-1,4-BDC MOF. On the other hand, for Ce-1,2,4-BTC MOF and Ce-1,2,4,5-BTEC MOF it is not discernible. This leads to a contrast of carbon content in different samples apart from varying carbon content in different organic linkers. The origin of this phenomenon is still unknown and not clear to us. A probable explanation can be given on basis of reduction of CeO_2: During the inert calcination process, the in situ synthesized carbons (derived from organic linkers) act as reducing agent.

The onset of auto-combustion process depends on the amount of unstable reduced cerium oxide present in the sample.

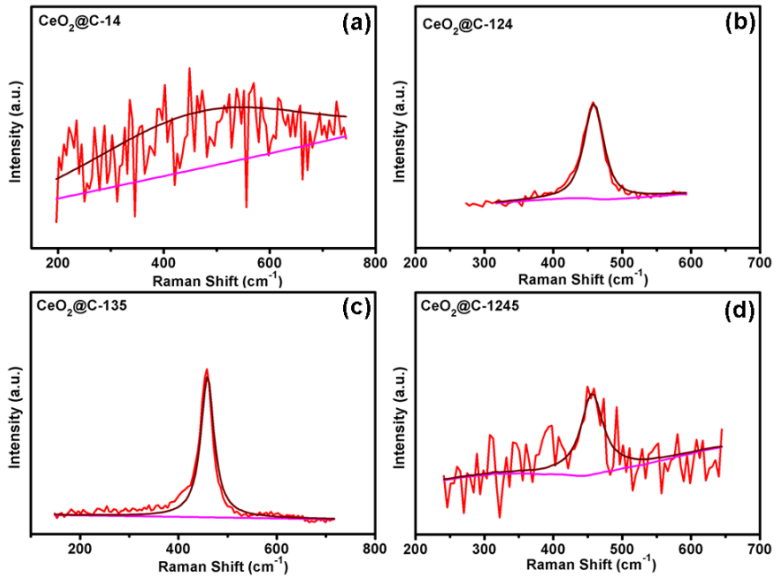

Fig. S3. Raman shift of CeO_2 of the synthesized samples (a) CeO_2@C -14, (b) CeO_2@C -124, (c) CeO_2@C -135 and (d) CeO_2@C -1245

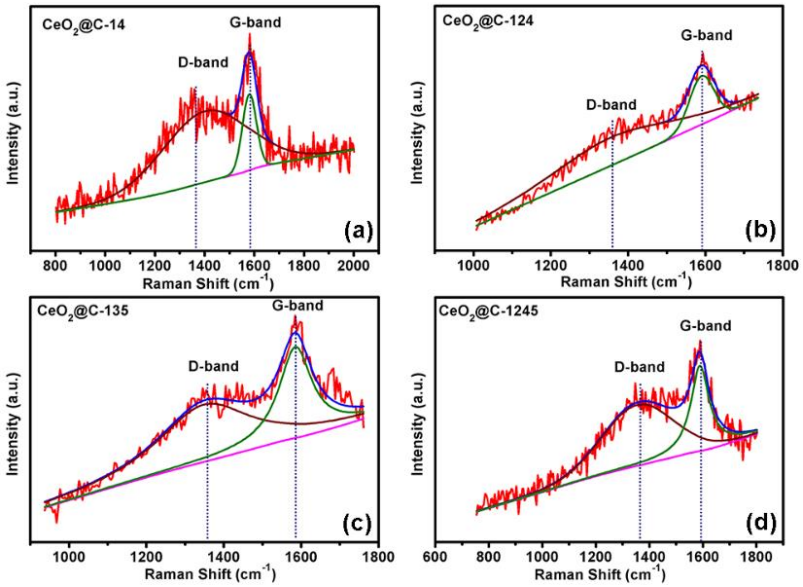

Fig. S4. Raman shift of carbon matrix generated from inert calcination of organic linkers of the synthesized samples (a) CeO_2@C -14, (b) CeO_2@C -124, (c) CeO_2@C -135 and (d) CeO_2@C -1245

Table-S2. Raman spectroscopy data

Sample ID	I_D/I_G	La (nm)	υ (I_D) (cm^{-1})	$\Delta\upsilon$ (I_D) (cm^{-1})	υ (I_G) (cm^{-1})	$\Delta\upsilon$ (I_G) (cm^{-1})	υ (I_{Ce}) (cm^{-1})	$\Delta\upsilon$ (I_{Ce}) (cm^{-1})
CeO_2@C-14	5.8	25.52	1359	09	1581	01	457	03
CeO_2@C-124	3.7	16.28	1360	10	1590	10	459	01
CeO_2@C-135	1.65	7.26	1357	07	1585	05	458	02
CeO_2@C-1245	1.95	8.58	1352	02	1589	09	457	03

I_D/I_G = Relative concentration of disorder and graphitic carbon; La = lateral dimension; υ = Raman Shift value; $\Delta\upsilon$ = up/downshifting in Raman shift value.

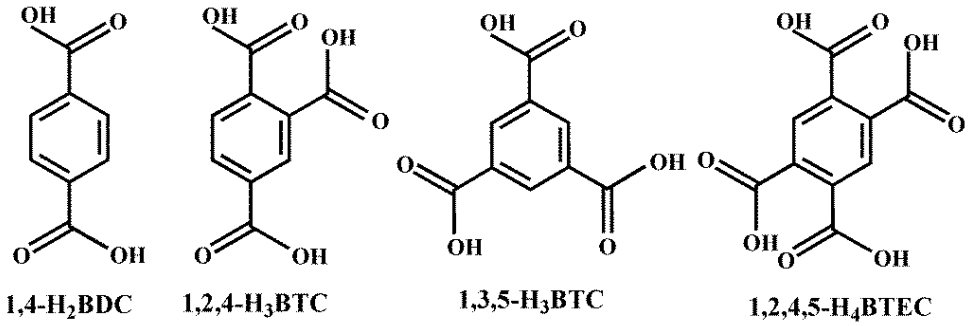

Fig. S5. Molecular structures of 1,4-benzenedicarboxylic acid (1,4-H_2BDC), 1,2,4-benzenetricarboxylic acid (1,2,4-H_3BTC), 1,3,5-benzenetricarboxylic acid (1,3,5-H_3BTC), 1,2,4,5-benzenedicarboxylic acid (1,2,4,5-H_4BTEC)

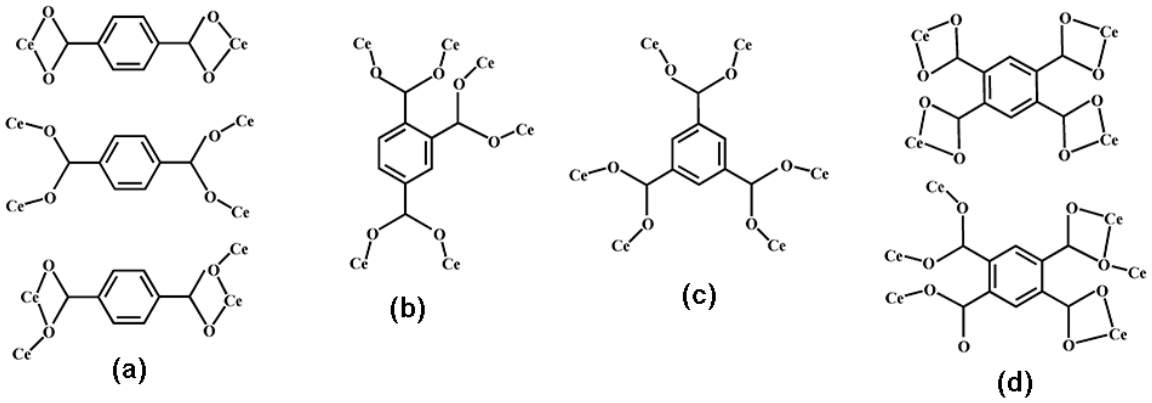

Fig. S6. Possible metal-ligand co-ordinations in the Ce-MOFs synthesized here.

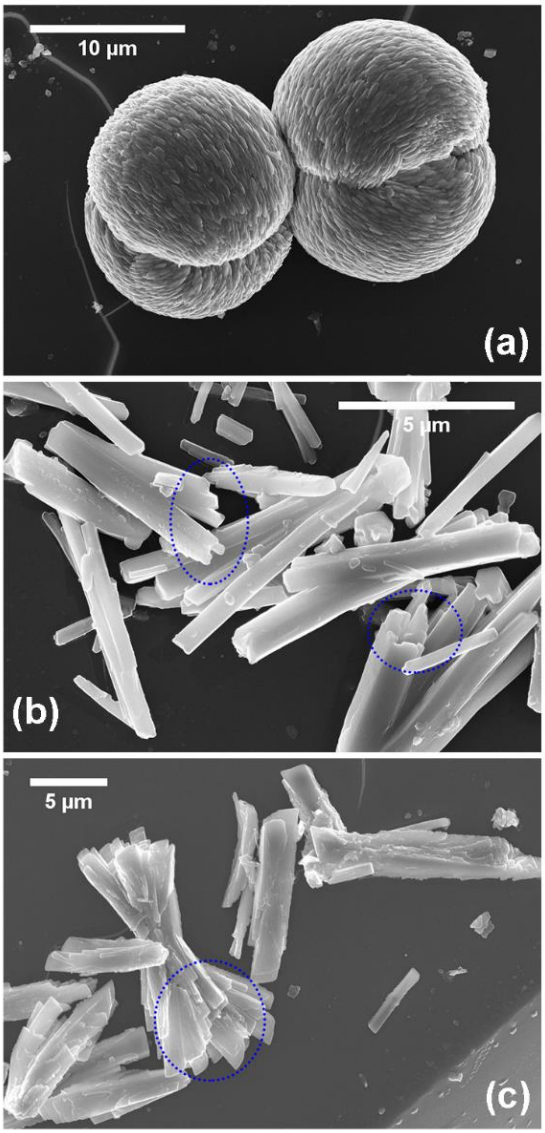

Fig. S7. FESEM micrographs showing assembly of (a) Ce-1,2,4-BTC spheres (b) Assembly of Ce-1,3,5-BTC macro bars (circled) and (c) Ce-1,2,4,5-BTEC macro plates (circled)

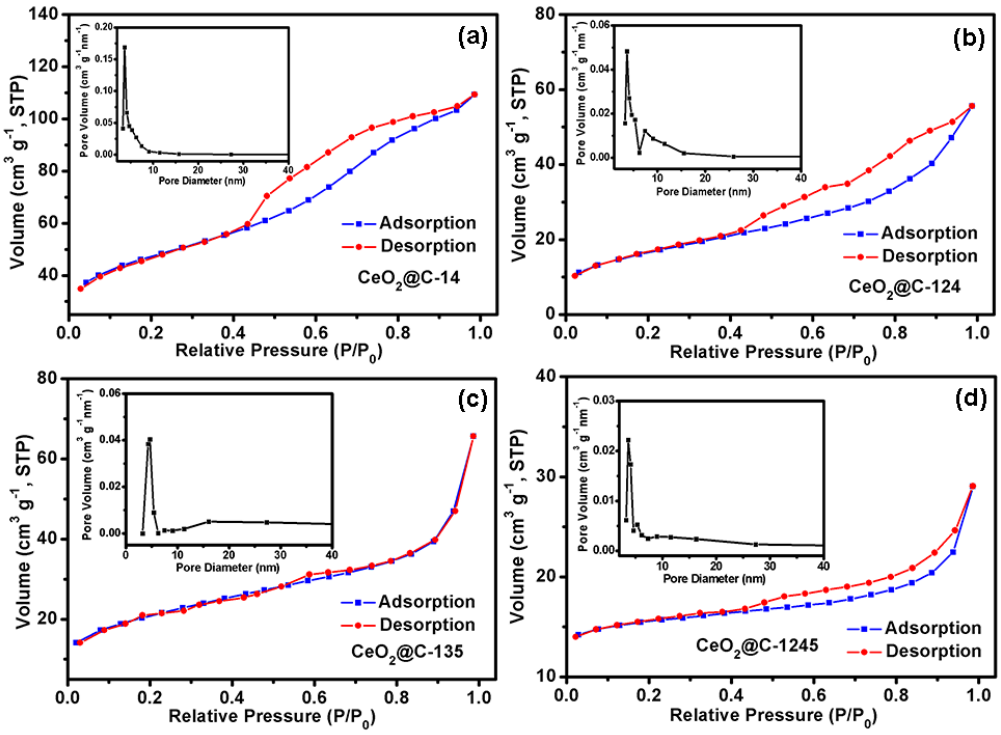

Fig. S8. N_2 adsorption-desorption isotherms and corresponding pore size distributions (insets) of CeO_2@C-14 (a), CeO_2@C-124 (b), CeO_2@C-135 (c) and CeO_2@C-1245 (d).

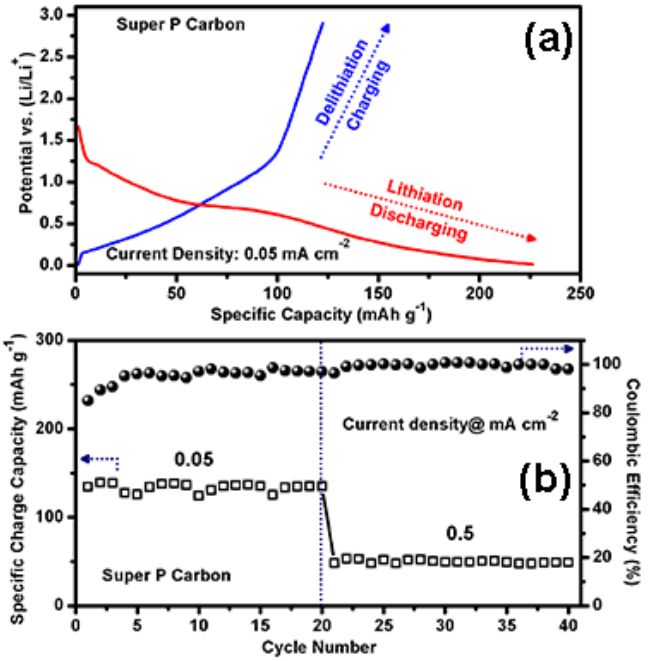

Fig. S9. Electrochemical properties of Super P carbon: (a) initial discharge-charge cycle and (b) cycling performance at two current densities of 0.05 and 0.5 mA cm^{-2}

In order to investigate the contribution of Super P, if any, we have conducted electrochemical tests using Super P carbon as a negative electrode material in a weight ratio of 90:10 (Super P Carbon : PVDF). The initial discharge-charge cycle and cyclic performance at two different current densities are shown in Fig.S9. During the cycling performance, at a low current density of 0.05 mA cm^{-2}, the specific charge capacity has been found to be 135 mAh g^{-1} after 20 cycles. When the current density is increased to a relatively higher value of 0.5 mA cm^{-2}, the specific capacity drops to 49 mAh g^{-1}. As the CeO_2@C electrodes contains only 20% of Super P Carbon, the overall contribution to its capacity (674 mAh g^{-1} at 0.05 mA cm^{-2} and 453 mAh g^{-1} at 0.5 mA cm^{-2}) is only 4.0% at 0.05 mA cm^{-2} and 2.1% at 0.5 mA cm^{-2}.

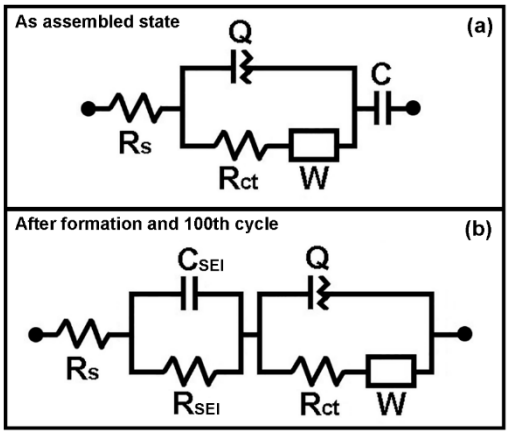

Fig. S10. Equivalent circuit models (a) as assembled state (b) after formation and 100th discharge-charge cycle.

Table-S3. Reported LIB results on CeO_2

Material	Voltage (V vs. Li/Li^+)	Current Density (mA cm^{-2})	Current Density (mA g^{-1}/ C rate)	Specific Capacity (mAh g^{-1})	Cycling performance	Ref.
CeO_2 Sphere	0.1-2.5	0.5 mA cm^{-2}	-	430	40 cycles	[1]
CeO_2 Sphere	0.1-3.0	-	0.1 C	530	50 cycles	[2]
CeO_2-graphene	0.001-3.0	-	50 mA g^{-1}	605	100 cycles	[3]
CeO_2@C	0.0-3.0	-	0.2 C	355	50 cycles	[4]
Brick like CeO_2	0.1-2.5	-	200 mA g^{-1}	460	100 cycles	[5]
Plate like CeO_2	0.1-2.5	-	200 mA g^{-1}	290	100 cycles	[5]
Rhombus CeO_2	0.1-2.5	0.2 mA cm^{-2}	-	374	50 cycles	[6]

Core-shell sphere CeO_2	0.1-2.5	0.2 mA cm^{-2}	-	547	300 cycles	[7]
Graphene/CMK-3 /CeO_2	0.01-3.0	-	0.1 A g^{-1}	550	100 cycles	[8]
Prism-like CeO_2 microrods	0.01-1.5	0.2 mA cm^{-2}	-	319.5	100 cycles	[9]
Micro/nano dumbbell-shaped CeO_2	0.1-2.5	0.2 mA cm^{-2}	-	590	100 cycles	[10]
Core-shell CeO2 micro/nanospheres	0.01-1.5	0.2 mA cm^{-2}	-	327	100 cycles	[11]
MOF-derived spherical CeO_2@C-14	0.01-3.0	0.05 mA cm^{-2} 0.1 mA cm^{-2} 0.5 mA cm^{-2}	-	674 590 453	100 cycles	[This work]

References

[1] F. Zhou, X. Ni, Y. Zhang and H. Zheng, *J. Colloid Interface Sci.*, 2007, **307**, 135-138.

[2] F. Zhou, X. Zhao, H. Xu, and C. Yuan, *J. Phys. Chem. C*, 2007, **111**, 1651-1657.

[3] G. Wang, J. Bai, Y. Wang, Z. Rena and J. Baic, *Scripta Mater.*, 2011, **65**, 339-342.

[4] X. Wu, H. Niu, S. Fu, J. Song, C. Mao, S. Zhang, D. Zhang and C. Chen, *J. Mater. Chem. A*, 2014, **2**, 6790-6795.

[5] H. Pang and C. Chen, *RSC Adv.*, 2014, **4**, 14872-14878.

[6] H. Liu and Q. Le, *J. Alloys Compd.*, 2016, **669**, 1-7.

[7] H. Liu and H. Liu, *Mater. Lett.*, 2016, **168**, 80-82.

[8] R. Guo, W. Yue, Y. Ren and W. Zhou, *Mater. Res. Bull.*, 2016, **73**, 102-110.

[9] C. Cheng, F. Chen, H. Yi and G. Lai, *J. Alloys Compd.*, 2017, **694**, 276-281.

[10] H. Liu, H. Liu, *J. Alloys Compd.*, 2016, **681**, 342-349.

[11] H. Liu, H. Liu, X. Han, *J. Solid State Electrochem.*, DOI 10.1007/s10008-016-3320-6